# Atomic resolution structure of a DNA-binding histone protein from the bacterium *Bdellovibrio bacteriovorus*

**Yimin Hu[a], Silvia Deiss[a], Joe D. Joiner[a], Marcus D. Hartmann[a,b], Andrei N. Lupas[a], Birte Hernandez Alvarez[a,*], Vikram Alva[a,*]**

[a]Department of Protein Evolution, Max Planck Institute for Biology Tübingen, Tübingen 72076, Germany
[b]Interfaculty Institute of Biochemistry, University of Tübingen, Tübingen, Germany

*To whom correspondence should be addressed
E-mail: birte.hernandez@tuebingen.mpg.de or vikram.alva@tuebingen.mpg.de

**Abstract**

Histones are DNA-binding proteins that play a crucial role in DNA packaging and gene regulation in eukaryotes and archaea. In eukaryotes, histones form octamers that constitute the core of the nucleosome, the fundamental unit of chromatin. Archaeal histones, on the other hand, form tetramers that assemble into extended superhelices upon DNA binding. Although previously thought to occur only in archaea and eukaryotes, histone homologs have recently been discovered in bacteria. This work presents the dimeric crystal structure of the bacterial histone HBb from *Bdellovibrio bacteriovorus* determined at a resolution of 1.06 Å, representing the first-ever structure of any histone protein determined at atomic resolution. Furthermore, this study shows that HBb binds DNA and is essential for bacterial viability, suggesting that bacterial histone homologs likely have a similar biological function as their eukaryotic and archaeal counterparts. These findings have important implications for our understanding of the fundamental processes of DNA organization and regulation in all domains of life.

**Keywords:** Histone; Histone fold; Nucleosome; Chromatin; *Bdellovibrio bacteriovorus*; DNA binding; Crystal structure; Atomic resolution

## 1. Introduction

Histones are a class of highly conserved DNA-binding proteins found in archaea and eukaryotes. They exhibit a characteristic fold, referred to as the histone fold, which comprises three α-helices connected by two short strap loops (Arents *et al.*, 1991, Luger *et al.*, 1997). In eukaryotes, the four core histones (H2A, H2B, H3, and H4) assemble into an octamer that wraps around approximately 146 base pairs of double-stranded DNA to form the nucleosome, which is the fundamental unit of chromatin (Arents *et al.*, 1991, Kornberg & Thomas, 1974, Luger *et al.*, 1997). A distinctive feature of eukaryotic histones is their unstructured N-terminal tails, which serve as hotspots for post-translational modifications and determine the function of histones in various cellular processes, including transcriptional regulation, DNA repair, replication, and condensation (Jenuwein & Allis, 2001, Luger & Richmond, 1998).

Until the discovery of the first archaeal histone homologs, HMfA and HMfB, in the hyperthermophilic archaeon *Methanothermus fervidus*, histones were thought to occur exclusively in eukaryotes (Sandman *et al.*, 1990). HMfA and HMfB exhibit the histone fold and assemble into tetramers that wrap DNA, forming elongated nucleosome-like structures (Bhattacharyya *et al.*, 2018, Mattiroli *et al.*, 2017). Following the initial discovery of histones in archaea, further homologs - usually one or two copies - have been found in most archaeal lineages (Ammar *et al.*, 2012, Maruyama *et al.*, 2013, Pereira *et al.*, 1997, Reeve *et al.*, 1997, Sandman & Reeve, 2000, 2006, Sanders *et al.*, 2021), including the Asgard superphylum, whose members are the closest prokaryotic relatives of eukaryotes (Henneman *et al.*, 2018, Stevens *et al.*, 2020). Archaeal histones assemble both into homo- and hetero-oligomers and have varying sizes, with some even possessing N- or C-terminal tails similar to eukaryotic histones (Henneman *et al.*, 2018, Stevens & Warnecke, 2023). This diversity observed in archaeal histones suggests that they serve distinct roles in genome organization and regulation (Peeters *et al.*, 2015, Sanders *et al.*, 2021, Stevens *et al.*, 2020, Kouzarides, 2007).

Historically, it was widely believed that bacteria lacked histone homologs, and the few instances of histones observed in bacteria were thought to have been acquired through horizontal gene transfer (Alva *et al.*, 2007, Qiu *et al.*, 2006). To shed light on the origin of histones and nucleosome-based DNA packaging and regulation, we recently conducted a systematic search for histones in bacteria and discovered about 600 histone homologs scattered sparsely across diverse bacterial classes, including Actinomycetes, Aquificae, Bacteroidia, Chlamydiia, Chloroflexia, Cyanophyceae, Deinococci, Elusimicrobia Oligoflexia, and Spirochaetia (Alva & Lupas, 2019). Through sequence and structure analysis, we classified these homologs into two groups: the pseudodimeric group, which consists of two consecutive copies of the histone domain on a single chain, and the single histone fold group, which comprises only one copy. We found that many bacterial histones exhibit conserved residues that are critical for DNA binding in eukaryotic and archaeal histones (Fig. 1). Thus, we proposed that bacterial

histones also bind DNA and that their origin dates back to the time of the last universal common ancestor (Alva & Lupas, 2019).

In this study, we present the crystal structure and biochemical characterization of the histone homolog HBb from the predatory proteobacterium *Bdellovibrio bacteriovorus*. Our findings demonstrate that HBb forms a homodimer and has the ability to bind DNA. Moreover, our findings also show that HBb is essential for maintaining bacterial viability. These results are consistent with a recent preprint published on bioRxiv, which reports the structure of the HBb-DNA complex and proposes a role for HBb in genome organization (Hocher *et al.*, 2023).

## 2. Materials and methods

### 2.1. Strains and plasmids

Cloning procedures using plasmids pUC57 and pETHis1a (Bogomolovas *et al.*, 2009) were performed in *Escherichia coli* Top10 cells. The gene encoding HBb (*BD_RS00255*, old locus tag: *Bd0055*) was codon-optimized and synthesized (BioTech, China) to be cloned into pETHis1a for recombinant expression of HBb (UniProt entry Q6MRM1) with an N-terminal $(histidine)_6$ tag using *E. coli* Mutant56(DE3) strain (Baumgarten *et al.*, 2017) as the expression host. *Bdellovibrio bacteriovorus* HD100 (DSM 50701, DSMZ, Germany) was cultured at 30 °C using *E. coli* Top10 as prey cells. For chromosomal deletion of *BD_RS00255* in *B. bacteriovorus*, the suicide vector pT18mobSacB was used. pT18mobsacB was a gift from Brian Kvitko (Addgene plasmid # 72648; http://n2t.net/addgene:72648; RRID: Addgene 72648).

### 2.2. Media

*E. coli* cells were grown on Luria-Bertani (LB) medium optionally supplemented with antibiotics. *B. bacteriovorus* was cultured in PYE broth, which was also optionally supplemented with antibiotics.

### 2.3. Expression and purification of HBb

*E. coli* MutantM56(DE3) cells harboring pETHis1a-HBb were cultivated in LB broth, supplemented with kanamycin at 37 °C. At an $OD_{600}$ of 0.5, IPTG was added to the cultures at a final concentration of 1 mM to induce protein expression. After further cultivation for 4 hours, cells were harvested by centrifugation.

All purification steps were performed at 4 °C, and 5 mM 2-mercaptoethanol was added to all buffers to prevent cysteine disulfide bridge formation. The cell pellet was resuspended in a buffer containing 20 mM Tris, pH 8.0, 300 mM NaCl, 1 M urea, 10 mM imidazole, supplemented with 1x protease inhibitor (cOmplete™, EDTA-free Protease Inhibitor Cocktail, Roche, Germany), 0.1 mM PMSF, 3 mM $MgCl_2$, and DNase. Cells were lysed by sonication for 15 minutes. Cell debris and membranes were

pelleted at 95,000 x g for 45 minutes. The supernatant was filtered with a 0.45 µm filter and applied on a 5 mL HisTrap column (Cytiva, US). The bound proteins were eluted with a linear gradient of 10-500 mM imidazole in the aforementioned buffer. The N-terminal tag was cleaved by incubating the HBb-containing fractions with histidine-tagged TEV protease. Following a second HisTrap column to remove TEV, HBb was purified to homogeneity by gel filtration chromatography on a Superdex 75 column (Cytiva, US) equilibrated with 20 mM Tris, pH 8.0, 150 mM NaCl, 1 M urea. Protein purity was assessed using SDS-PAGE (15 %) and BN-PAGE (4-16%, ThermoFisher Scientific, US) and protein concentration was determined using the BCA protein assay (ThermoFisher Scientific, US).

### 2.4. Circular dichroism (CD) spectroscopy

HBb was diluted in 20 mM Tris, pH 8.0, 1 M urea to a final concentration of 0.4 mg/mL. CD spectra were measured with a Jasco J-810 spectrometer (JASCO, Japan) in a wavelength range of 200-250 nm, using a cuvette with a path length of 1 mm and a read speed of 100 nm/min. A total of three single spectra were recorded and averaged. To analyze the thermal stability of HBb, the ellipticity (θ) was measured at 220 nm over a temperature gradient of 20-90 °C applying a ramp of 1 °C/min, a data pitch of 0.5, and a response time of 1 s. Data analysis was performed using the Spectra Manager software suite (JASCO, Japan). CD spectra and the melting curve were plotted using Prism 9 (GraphPad, US).

### 2.5. Size exclusion chromatography coupled with multi-angle light scattering (SEC-MALS)

HBb at a concentration of 3 mg/mL was incubated on ice for 20 minutes before loading onto a Superdex 75 Increase 10/300 GL column (Cytiva, US), equilibrated with 20 mM Tris pH 8.0, 150 mM NaCl, 1 M urea. The run was performed at a flow rate of 0.5 mL/min on a 1260 Infinity II HPLC system (Agilent, US) coupled to a miniDAWN TREOS and Optilab T-rEX refractive index detector (Wyatt Technology, US). HBb was detected at 215 nm. Molar mass distributions were calculated using the ASTRA v.7.3.0.18 software suite (Wyatt Technology, US).

### 2.6. Crystallization, data collection, and structure determination

Crystallization was set up in 96-well sitting-drop vapor-diffusion plates using commercially available screens. Crystals grew under multiple conditions within 1-3 days and the best-diffracting crystals were obtained under the conditions listed in Table 1. Crystals were transferred into a droplet of reservoir solution supplemented with 10% (v/v) PEG 400 for cryo-protection, loop-mounted and flash-cooled in liquid nitrogen. Data were collected at beamline X10SA of the Swiss Light Source (Villigen, Switzerland) at 100 K, using an EIGER X 16M hybrid pixel detector (Dectris Ltd., Switzerland). Data were reduced, processed and scaled in space group $P2_12_12$ to a resolution of 1.06 Å using XDS (Kabsch, 2010) with the

statistics listed in Table 2. The structure was solved by molecular replacement using Phaser (McCoy, 2007) and HMk (PDB entry 1F1E) as a search model, locating one monomer of the protein in the asymmetric unit. The structure was rebuilt and refined in cycles with manual modelling in Coot (Emsley & Cowtan, 2004) and refinement with REFMAC5 (Murshudov *et al.*, 2011) with the statistics listed in Table 3. The structure was deposited in the PDB under accession code 8CMP.

### 2.7. Electrophoretic mobility shift assay (EMSA)

*In vitro* DNA-binding tests were performed using pUC19 linearized with *Hin*dIII and a 90-bp DNA fragment amplified from pUC19. In brief, a defined quantity of DNA was mixed with increasing amounts of protein sample in 25 mM Tris pH 8.0, 125 mM NaCl, 100 mM KCl, 1 M urea and incubated at 37 °C for 10 min. Samples with pUC19 DNA were separated on 0.8 % agarose gels, samples with shorter fragments were analyzed using 10 % TBE native gels. Fragments were visualized by SYBR Gold staining (ThermoFisher Scientific, US).

### 2.8. Microscale thermophoresis (MST)

For the MST experiments, an 80-bp DNA fragment was used that was reported to have a high binding affinity to HMfB (Bailey *et al.*, 2000, Mattiroli *et al.*, 2017). Accordingly, oligonucleotides Cy5-HHA-F and HHA-R with the sequences ’[cyanine5]-CCGTACTGTCGTCTGCGGCCTTTGATTATCAATTAAAGCGTTCTACGGCGTTTTTGATCGCTCAACGTGCGGAGCTAGAT)-3’ and 5’-ATCTAGCTCCGCACGTTGAGCGATCAAAAACGCCGTAGAACGCTTTAATTGATAATCAAAGGCCGCAGACGACAGTACGG-3’ were synthesized (Merck, Germany) and annealed by incubation at 95 °C for 5 minutes, followed by slow cooling to RT. A dilution series of the label-free protein sample was prepared in 20 mM Tris, pH 8.0, 150 mM NaCl, 1 M urea and titrated against the annealed Cy5-labeled DNA fragment *hha* at the concentration of 20 nM. Samples were incubated at 37 °C for 10 minutes, centrifuged to remove precipitates, and loaded into Monolith NT ‘Premium coated’ capillaries. Measurements were performed using the Monolith NT.115 instrument, repeated in triplicate and analyzed using MO.Control (NanoTemper Technologies, Germany).

### 2.9. Deletion of BD_RS00255

For the deletion of *BD_RS00255* (old locus tag: *Bd0055*) in *B. bacteriovorus* HD100, a previously described method was used with slight modifications (Hobley *et al.*, 2012, Roschanski *et al.*, 2011). Briefly, the suicide vector pT18mobSacB harboring a kanamycin resistance cassette flanked by the genomic regions upstream and downstream of *BD_RS00255* (nucleotides 47964-49345 and 49567-50958 of the complete genome of *B. bacteriovorus* strain HD100; segment 1/11, Sequence ID: BX842646.1)

was introduced into *B. bacteriovorus* via conjugation. Chromosomal integration of the plasmid by homologous recombination was verified by PCR and sequencing. To select for a second crossover event resulting in the replacement of *BD_RS00255* by the kanamycin resistance cassette, cells were grown on medium containing 5-10 % sucrose.

## 3. Results and discussion

### 3.1. Biophysical properties of the histone protein HBb from *B. bacteriovorus*

To investigate the structure and function of bacterial histones, we decided to experimentally characterize the histone protein HBb of *B. bacteriovorus* (UniProt entry Q6MRM1). This protein consists of only 64 amino acid residues and features a single histone fold domain. We selected *B. bacteriovorus* as a model organism because it is one of the few histone-containing bacteria that can be cultured, and because it has established tools for genetic manipulation. After overexpressing HBb in *E. coli* and purifying it to homogeneity, we confirmed the purity of the protein using SDS-PAGE, which showed a single band with a molecular weight of 10 kDa, consistent with the theoretical molecular weight of 7 kDa (Fig. 2a). Separation of the protein by BN-PAGE revealed two bands, a major and a smaller band of lower molecular weight, which could suggest different types of oligomers (Fig. 2a). However, further analysis of HBb by SEC-MALS showed only one major peak with a calculated molecular weight of 14 kDa, corresponding to a dimer (Fig. 2b). CD spectroscopy analysis revealed that HBb is an α-helical protein with flexible regions, which undergoes cooperative unfolding when heated with a melting temperature (Tm) of 51.6 °C (Fig. 2c).

### 3.2. Crystal structure of HBb

Using a vapor-diffusion setup, we obtained crystals of HBb in space group $P2_12_12$ that diffracted to atomic resolution within a few days. The diffraction data were processed to a resolution of 1.06 Å, and the structure (PDB entry 8CMP) was solved by molecular replacement using the archaeal histone HMk (PDB entry 1F1E) as a search model. The asymmetric unit contains only a single chain of HBB, forming a dimer by crystallographic symmetry. Apart from the first three and last three amino acids, the full chain is clearly resolved in the electron density map. Notably, our structure is the first-ever atomic resolution structure of a histone protein; the previous highest resolution (1.48 Å) structure was that of histone HMfA from *M. fervidus* (PDB entry 1B67) (Decanniere *et al.*, 2000).

HBb exhibits a characteristic dimeric histone fold, with monomers consisting of three α-helices (α1, α2, α3) connected by two loops (l1 and l2) (Fig. 2d). In each monomer, the longer central helix α2 is flanked at both ends by the shorter helices α1 and α3. Dimerization occurs through the antiparallel

alignment of the central α2-helices of the two monomers at an angle of about 25°. The dimer is stabilized mainly by hydrophobic contacts along the interface, involving residues L31, I35, and L38 in α2, in addition to contributions from α1 (e.g., V11) and α3 (e.g., I59). Compared to the archaeal histone homolog HMfB (Fig. 2e), the α2-helix of HBb is one turn shorter, whereas α3 consists of only a single helical turn.

A comparison of the HBb and HMfB sequences indicates that residues involved in the tetramerization of HMfB (Marc *et al.*, 2002, Stevens *et al.*, 2020) are not present in HBb (Fig. 1), suggesting that the crystallographic dimer of HBb probably represents the physiological oligomer. Like HMfB, HBb also has a highly conserved intramolecular salt bridge, the RD clamp, located in loop l2 and formed by residues R51 and D58 (Fig. 2d). In HBb, this motif is extended by D49, which forms an additional salt bridge with R51. This extended RD clamp may provide increased stability to the conserved KT motif in loop I2, which mediates DNA contacts in HMfB. Of the six residues known to mediate DNA binding in HMfB, four, including K52 and T53, are conserved in HBb (Fig. 1). This suggests that HBb likely binds DNA, but possibly in a different manner than HMfB. Indeed, an HBb-DNA complex reported in a recent preprint suggests that HBb binds DNA differently than archaeal and eukaryotic histones (Hocher *et al.*, 2023).

### 3.3. HBb binds DNA in vitro and is essential for growth

To investigate the potential interaction between HBb and DNA, we performed EMSA using both a 2686-bp linearized plasmid pUC19 and a shorter 80-bp DNA fragment. We observed a characteristic band shift, indicating complex formation between HBb and the DNA fragments (Fig. 3a, b). In addition, we used MST to determine the binding affinity of HBb to an 80-bp DNA fragment, which was found to be $K_d$ = 39.5 ± 3.6 µM (Fig. 3c). This value is considerably lower than the nanomolar DNA-binding affinities determined for other histone homologs (Bailey *et al.*, 2002, Marc *et al.*, 2002), indicating that HBb likely binds to DNA non-specifically via a different type of interaction, as was shown recently (Hocher *et al.*, 2023).

Previous studies have demonstrated that the *hbb* gene expression is induced during the highly replicative *B. bacteriovorus* growth phase, which is associated with prey consumption (Karunker *et al.*, 2013). To understand the functional significance of HBb, we attempted to construct a strain in which the *hbb* gene (*BD_RS00255*) was replaced by a kanamycin resistance cassette. However, we were unable to select for the loss of the gene, suggesting that HBb is essential for *B. bacteriovorus* during the growth phase, as also shown in a recent study (Hocher *et al.*, 2023). These results provide compelling evidence for the critical role of HBb in the growth and survival of *B. bacteriovorus*.

## 4. Summary

We recently discovered histone proteins in many different classes of bacteria, leading us to hypothesize that they may play a role in DNA packaging and gene regulation in bacteria (Alva & Lupas, 2019). In this study, we investigated this hypothesis by solving the crystal structure and examining the DNA-binding properties of the histone protein HBb of *B. bacteriovorus*. Our results show that, like histones found in archaea and eukaryotes, HBb exhibits the characteristic histone fold, oligomerizes, and binds DNA. However, unlike archaeal and eukaryotic histones, recent research has shown that HBb does not form nucleosome-like structures, but that HBb dimers form a sheath around straight DNA (Hocher *et al.*, 2023). Futhermore, we found that HBb is indispensable for the survival of *B. bacteriovorus*, suggesting that bacterial histones, much like their counterparts in archaea and eukaryotes, are likely involved in critical cellular functions. However, further studies are necessary to fully explore and understand these potential functions.

## Acknowledgements

We thank Reinhard Albrecht and Antoine Schramm for assistance with crystallization, crystallographic data collection and processing, and the staff of beamline X10SA of the Swiss Light Source (PSI, Villigen, Switzerland) for excellent technical support. This work was supported by institutional funds of the Max Planck Society.

```
Eukaryotic histones          hhhhhhhhhhhh        hhhhhhhhhhhhhhhhhhhhhhhhhh      hhhhhhhhhh
H. sapiens (H2A)      [28]   VGRVHRLLRKGNYSERVGAGAPVYLAAVLEYLTAEILELAGNAARDNKKTRIIPRHLQLAIRN
H. sapiens (H2B)      [39]   SVYVYKVLKQVHPDTGISSKAMGIMNSFVNDIFERIAGEASRLAHYNKRSTITSREIQTAVRL
H. sapiens (H3)       [69]   QRLVREIAQDFKTDLRFQSSAVMALQEACEAYLVGLFEDTNLCAIHAKRVTIMPKDIQLARRI
H. sapiens (H4)       [32]   KPAIRRLARRGGVK-RISGLIYEETRGVLKVFLENVIRDAVTYTEHAKRKTVTAMDVVYALKR

Archaeal histones            hhhhhhhhhh        hhhhhhhhhhhhhhhhhhhhhhhhhh       hhhhhhhhhh
M. fervidus (HMfA)    [6]    IAPIGRIIKNAGAE-RVSDDARIALAKVLEEMGEEIASEAVKLAKHAGRKTIKAEDIELARKM
M. fervidus (HMfB)    [5]    IAPIGRIIKDAGAE-RVSDDARITLAKILEEMGRDIASEAIKLARHAGRKTIKAEDIELAVRR

Bacterial histones           hhhhhhhhhhhh      hhhhhhhhhhhh    hhhhhhhhhhhhh      hhh
B. bacteriovorus (HBb)[8]    TSKVKKLIKEKGQMN-TSAETIDVLSKAIE----QLCLKGVESAKADGRKTVMARDIVIDHL-
L. interrogans        [14]   TSKVKAYIKSKGFM--TSGDAIDGLNDKIH----QLIDDAVKRTESNKRSTVRPTDF------
P. pacifica           [14]   GSKVKAIVRDAGL--RSDGELVAALSGRVH----AMLEGAIVRCTRNMRSTVRPQDL------
E. salina             [20]   GSKVKDVVRAAGY--RSDGELVQAVSEKVH----EMLEAAIKRAESNKRGTVRPYDL------
N. exedens            [15]   GSKVKDVIRDAGL--RSDGELIQAVSDKVH----ELLGAAIERCKSNNRSTVRPYDL------
```

**Figure 1. Sequence alignment of representative eukaryotic, archaeal, and bacterial histones.** Conserved residues are colored according to their properties characterized in archaeal and eukaryotic histones; residues involved in DNA binding are colored in orange, residues that play a role in tetramerization are colored in green, and the glycine residue important for the polymerization of HMfB is colored in magenta. UniProt/NCBI accession of shown sequences are: *Homo sapiens* (H2A - P04908; H2B - P62807; H3 - P68431; H4 - P62805), *M. fervidus* (HMfA - P48781; HMfB - P19267), *B. bacteriovorus* (Q6MRM1), *Leptospira interrogans* (Q8F3E8), *Plesiocystis pacifica* (A6GF99), *Enhygromyxa salina* (WP_052547863.1), and *Nannocystis exedens* (WP_096326703.1).

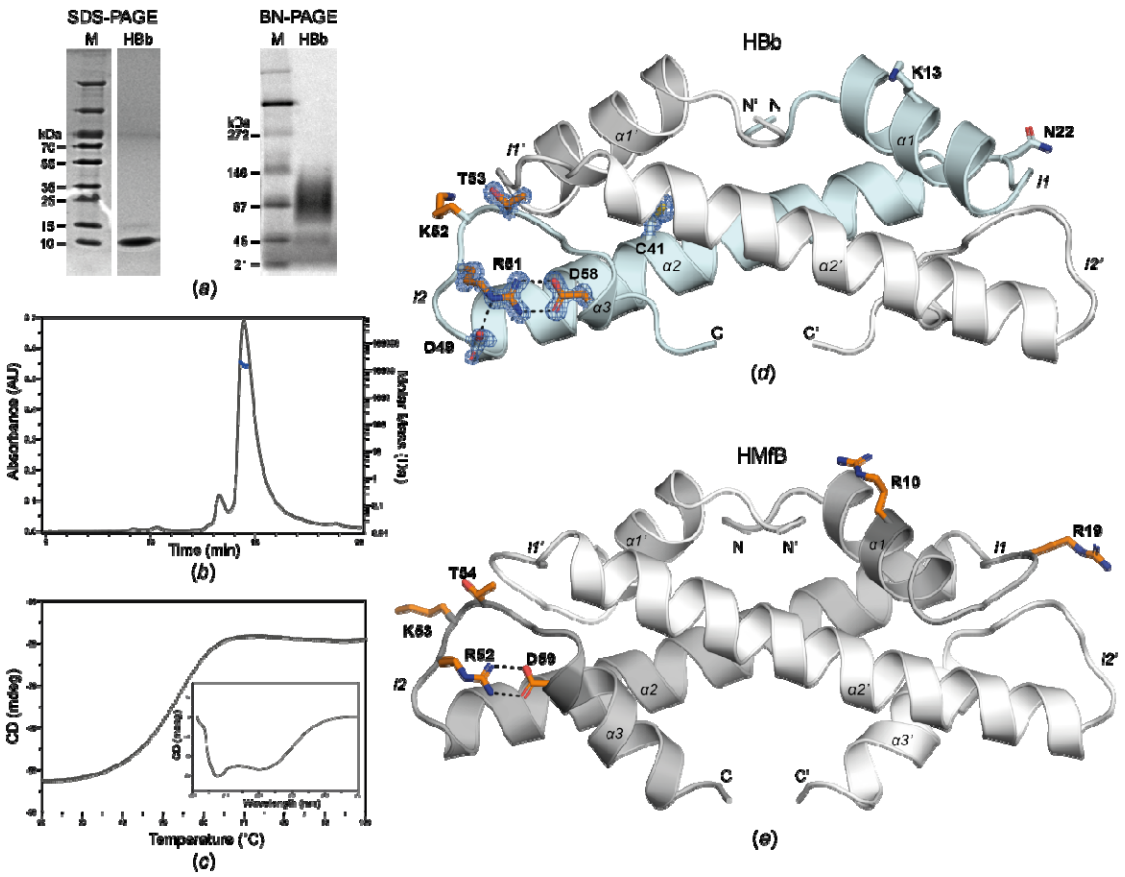


**Figure 2. Biophysical characterization of HBb.** (a) SDS-PAGE and BN-PAGE of purified HBb. (b) SEC-MALS profile of HBb. (c) Melting curve of HBb based on changes in the molar ellipticity (θ) at 220 nm, the far-UV CD spectrum of HBb is shown in the inset. (d) The crystal structure of the HBb dimer (PDB entry 8CMP) is shown in cartoon representation, with selected residues shown as sticks. Conserved residues predicted to be involved in DNA binding or stabilization of the histone fold are shown in orange, further residues mentioned in the text in light cyan, and salt bridges between D49, R51, and D58 indicated as dashed lines. A representative $2F_o - F_c$ electron density map is shown for selected residues at a contour level of at 2.0 σ. (e) The crystal structure of the HMfB dimer (PDB entry 1A7W) is shown for comparison, with conserved residues playing a role in DNA binding or stabilization of the histone fold shown as sticks.

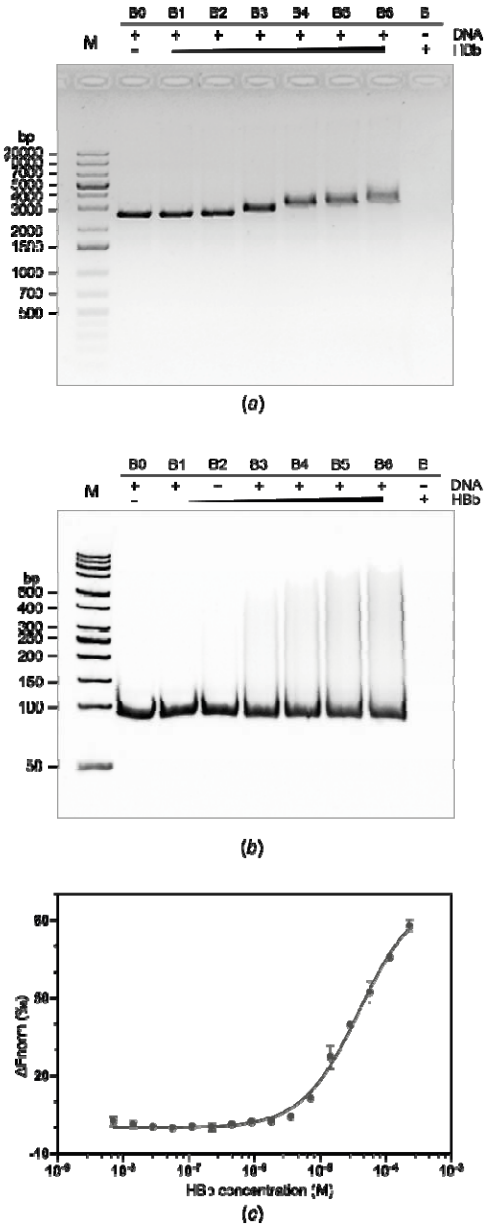


**Figure 3. Functional characterization of HBb.** (a) EMSA showing the binding of HBb to *Hin*dIII-linearized pUC19. Plasmid DNA at a concentration of 71 nM was incubated with increasing concentrations of HBb. The molar ratio of HBb (calculated assuming HBb exists exclusively as dimers) to DNA in lanes B1-B6 were 22:1, 187:2, 373:2, 549:2, 735:2 and 461:1. (b) EMSA showing the binding of HBb to a 90-bp DNA fragment amplified from pUC19. The 90-bp DNA fragment (683 nM) was incubated with increasing concentrations of HBb, respectively. The molar ratio of HBb (calculated assuming HBb exists exclusively as dimers) to 90-bp DNA in lanes B1-B6 were 1:2, 2:1, 31:8, 29:5, 31:4 and 29:3. (c) MST binding curve of HBb and *hha* DNA fragment (20 nM).

**Table 1 Crystallization conditions**

| | |
|---|---|
| Method | Sitting drop |
| Plate type | INTELLI-PLATE 96-3 |
| Temperature (K) | 293 |
| Protein concentration | 3 mg/mL |
| Buffer composition of protein solution | 20 mM Tris pH 8.0, 150 mM NaCl, 1 M Urea |
| Composition of reservoir solution | 0.1 M sodium acetate, pH 4.5 and 25% (w/v) PEG 3350 |
| Volume and ratio of drop | 600 nL, 1:1 |
| Volume of reservoir | 100 µL |

**Table 2 Data collection and processing**

Values for the outer shell are given in parentheses.

| | |
|---|---|
| Diffraction source | Swiss Light Source beamline X10SA |
| Wavelength (Å) | 1 Å |
| Temperature (K) | 100 K |
| Detector | DECTRIS EIGER X 16M |
| Crystal-detector distance (mm) | 135 |
| Rotation range per image (°) | 1 |
| Total rotation range (°) | 360 |
| Exposure time per image (s) | 0.1 |
| Space group | $P2_12_12$ |
| *a*, *b*, *c* (Å) | 34.47, 56.35, 26.70 |
| α, β, γ (°) | 90, 90, 90 |
| Mosaicity (°) | 0.143 |
| Resolution range (Å) | 28.17–1.06 (1.13–1.06) |
| Total No. of reflections | 250341 (11742) |
| No. of unique reflections | 23226 (3028) |
| Completeness (%) | 96.3 (79.4) |
| Redundancy | 10.8 (3.88) |
| $\langle I/\sigma(I)\rangle$ | 23.80 (1.66) |
| $CC_{1/2}$ | 1.00 (0.688) |
| $R_{meas}$ | 0.047 (0.921) |
| Overall *B* factor from Wilson plot ($Å^2$) | 16.9 |

**Table 3 Structure solution and refinement**

Values for the outer shell are given in parentheses. Ramachandran statistics determined by PROCHECK (Laskowski *et al.*, 1993)

| | |
|---|---|
| Resolution range (Å) | 28.19-1.06 (1.09-1.06) |
| Completeness (%) | 96.4 |
| No. of reflections, working set | 20904 (1110) |
| No. of reflections, test set | 1161 (59) |
| Final $R_{cryst}$ | 0.142 (0.363) |
| Final $R_{free}$ | 0.169 (0.379) |
| No. of non-H atoms | 473 |
| Protein | 444 |
| Water | 29 |
| R.m.s. deviations | |
| Bonds (Å) | 0.019 |
| Angles (°) | 1.421 |
| Average *B* factors (Å$^2$) | 18.5 |
| Protein | 17.6 |
| Water | 32.7 |
| Ramachandran plot | |
| Most favoured (%) | 98.1 |
| Allowed (%) | 1.9 |

## References


Alva, V., Ammelburg, M., Soding, J. & Lupas, A. N. (2007). *BMC Struct Biol* **7**, 17.

Alva, V. & Lupas, A. N. (2019). *Bioinformatics* **35**, 2349-2353.

Ammar, R., Torti, D., Tsui, K., Gebbia, M., Durbic, T., Bader, G. D., Giaever, G. & Nislow, C. (2012). *Elife* **1**, e00078.

Arents, G., Burlingame, R. W., Wang, B. C., Love, W. E. & Moudrianakis, E. N. (1991). *Proc Natl Acad Sci U S A* **88**, 10148-10152.

Bailey, K. A., Marc, F., Sandman, K. & Reeve, J. N. (2002). *J Biol Chem* **277**, 9293-9301.

Bailey, K. A., Pereira, S. L., Widom, J. & Reeve, J. N. (2000). *J Mol Biol* **303**, 25-34.

Baumgarten, T., Schlegel, S., Wagner, S., Low, M., Eriksson, J., Bonde, I., Herrgard, M. J., Heipieper, H. J., Norholm, M. H., Slotboom, D. J. & de Gier, J. W. (2017). *Sci Rep* **7**, 45089.

Bhattacharyya, S., Mattiroli, F. & Luger, K. (2018). *FEBS J* **285**, 3168-3174.

Bogomolovas, J., Simon, B., Sattler, M. & Stier, G. (2009). *Protein Expr Purif* **64**, 16-23.

Decanniere, K., Babu, A. M., Sandman, K., Reeve, J. N. & Heinemann, U. (2000). *J Mol Biol* **303**, 35-47.

Emsley, P. & Cowtan, K. (2004). *Acta Crystallogr D Biol Crystallogr* **60**, 2126-2132.

Henneman, B., van Emmerik, C., van Ingen, H. & Dame, R. T. (2018). *PLoS Genet* **14**, e1007582.

Hobley, L., Fung, R. K., Lambert, C., Harris, M. A., Dabhi, J. M., King, S. S., Basford, S. M., Uchida, K., Till, R., Ahmad, R., Aizawa, S., Gomelsky, M. & Sockett, R. E. (2012). *PLoS Pathog* **8**, e1002493.

Hocher, A., Laursen, S. P., Radford, P., Tyson, J., Lambert, C., Stevens, K. M., Picardeau, M., Sockett, R. E., Luger, K. & Warnecke, T. (2023). *bioRxiv*, 2023.2001.2026.525422.

Jenuwein, T. & Allis, C. D. (2001). *Science* **293**, 1074-1080.

Kabsch, W. (2010). *Acta Crystallogr D Biol Crystallogr* **66**, 125-132.

Karunker, I., Rotem, O., Dori-Bachash, M., Jurkevitch, E. & Sorek, R. (2013). *PLoS One* **8**, e61850.

Kornberg, R. D. & Thomas, J. O. (1974). *Science* **184**, 865-868.

Kouzarides, T. (2007). *Cell* **128**, 693-705.

Laskowski, R. A., Macarthur, M. W., Moss, D. S. & Thornton, J. M. (1993). *J Appl Crystallogr* **26**, 283-291.

Luger, K., Mader, A. W., Richmond, R. K., Sargent, D. F. & Richmond, T. J. (1997). *Nature* **389**, 251-260.

Luger, K. & Richmond, T. J. (1998). *Curr Opin Genet Dev* **8**, 140-146.

Marc, F., Sandman, K., Lurz, R. & Reeve, J. N. (2002). *J Biol Chem* **277**, 30879-30886.

Maruyama, H., Harwood, J. C., Moore, K. M., Paszkiewicz, K., Durley, S. C., Fukushima, H., Atomi, H., Takeyasu, K. & Kent, N. A. (2013). *EMBO Rep* **14**, 711-717.

Mattiroli, F., Bhattacharyya, S., Dyer, P. N., White, A. E., Sandman, K., Burkhart, B. W., Byrne, K. R., Lee, T., Ahn, N. G., Santangelo, T. J., Reeve, J. N. & Luger, K. (2017). *Science* **357**, 609-612.

McCoy, A. J. (2007). *Acta Crystallogr D Biol Crystallogr* **63**, 32-41.

Murshudov, G. N., Skubak, P., Lebedev, A. A., Pannu, N. S., Steiner, R. A., Nicholls, R. A., Winn, M. D., Long, F. & Vagin, A. A. (2011). *Acta Crystallogr D Biol Crystallogr* **67**, 355-367.

Peeters, E., Driessen, R. P., Werner, F. & Dame, R. T. (2015). *Nat Rev Microbiol* **13**, 333-341.

Pereira, S. L., Grayling, R. A., Lurz, R. & Reeve, J. N. (1997). *Proc Natl Acad Sci U S A* **94**, 12633-12637.

Qiu, Y., Tereshko, V., Kim, Y., Zhang, R., Collart, F., Yousef, M., Kossiakoff, A. & Joachimiak, A. (2006). *Proteins* **62**, 8-16.

Reeve, J. N., Sandman, K. & Daniels, C. J. (1997). *Cell* **89**, 999-1002.

Roschanski, N., Klages, S., Reinhardt, R., Linscheid, M. & Strauch, E. (2011). *J Bacteriol* **193**, 1745-1756.

Sanders, T. J., Ullah, F., Gehring, A. M., Burkhart, B. W., Vickerman, R. L., Fernando, S., Gardner, A. F., Ben-Hur, A. & Santangelo, T. J. (2021). *Front Microbiol* **12**, 681150.

Sandman, K., Krzycki, J. A., Dobrinski, B., Lurz, R. & Reeve, J. N. (1990). *Proc Natl Acad Sci U S A* **87**, 5788-5791.

Sandman, K. & Reeve, J. N. (2000). *Arch Microbiol* **173**, 165-169.

Sandman, K. & Reeve, J. N. (2006). *Curr Opin Microbiol* **9**, 520-525.

Stevens, K. M., Swadling, J. B., Hocher, A., Bang, C., Gribaldo, S., Schmitz, R. A. & Warnecke, T. (2020). *Proc Natl Acad Sci U S A* **117**, 33384-33395.

Stevens, K. M. & Warnecke, T. (2023). *Semin Cell Dev Biol* **135**, 50-58.